Multi gas sensors using one nanomaterial, temperature gradient, and machine learning algorithms for discrimination of gases and their concentration

Nguyen Xuan Thai[a,b,§] and Matteo Tonezzer[c,d,*,§], Luca Masera[e], Hugo Nguyen[f], Nguyen Van Duy[a,*] and Nguyen Duc Hoa[a]

[a] ITIMS, Hanoi University of Science and Technology, Hanoi, Viet Nam

[b] Vietnam Metrology Institute, 8 Hoang Quoc Viet Road, Hanoi, Vietnam

[c] IMEM-CNR, sede di Trento - FBK, Via alla Cascata 56/C, Povo (TN), Italy

[d] University of Trento, Via Calepina 14, Trento, Italy

[e] DISI, University of Trento, Via Sommarive 9, Povo, Trento, Italy

[f] Uppsala University, Department of Material Science, Uppsala, Sweden

Abstract

In this work, four identical micro sensors on the same chip with noble metal decorated tin oxide nanowires as gas sensing material were located at different distances from an integrated heater to work at different temperatures. Their responses are combined in highly informative 4D points that can qualitatively (gas recognition) and quantitatively (concentration estimate) discriminate all the tested gases. Two identical chips were fabricated with tin oxide (SnO_2) nanowires decorated with different metal nanoparticles: one decorated with Ag nanoparticles and one with Pt nanoparticles. Support Vector Machine was used as the "brain" of the sensing system. The results show that the systems using these multisensor chips were capable of achieving perfect classification (100 %) and good estimation of the concentration of tested

[*] Corresponding authors' email addresses: matteo.tonezzer@cnr.it (Matteo Tonezzer), nguyenvanduy@itims.edu.vn (Nguyen Van Duy)

[§] These authors contributed equally to the work.

gases (errors in the range 8-28 %). The Ag decorated sensors did not have a preferential gas, while Pt decorated sensors showed a lower error towards acetone, hydrogen and ammonia. Combination of the two sensor chips improved the overall estimation of gas concentrations, but the individual sensor chips were better for some specific target gases.

Keywords: Gas sensor, Nanowires, Tin oxide, Selectivity, Machine learning

1. Introduction

Detection of volatile compounds in different environments and conditions is increasingly important, due to the environmental pollution related to the rapid urbanization and industrialization in the world. In the field of health care, quality control of food and beverage [1], agriculture [2], security against terrorism [3], and medical diagnosis [4] gas detection and measurement gains also its importance.

After thick films and then thin films of metal oxide semiconductor (MOS) as gas sensing materials a new gas sensor generation based on MOS nanostructures emerges. Among the nanostructures used as sensing layer for gas sensors, one-dimensional nanowires (NWs) have attracted widespread attention of numerous research groups in the world due to their great advantages such as a high surface area-to-volume ratio, high charge-carrier concentration, high crystallinity, simple growth, and stability [5,6]. The main advantages of MOS nanostructures are high sensitivity to a wide range of gases and compounds, whereas their main drawbacks are poor selectivity and they normally require high operation temperature (of some hundreds °C). Many approaches have been used to solve these problems, such as surface decoration with catalytic nanoparticles (NPs) of noble metal [7,8], using hybrid nanostructures [9,10], integration of a micro-heater onto the sensor chips [11]. Using different sensing materials and/or applying different operating temperatures are also an approach for detecting different target gases [12-14]. Furthermore, tuning size and shape of MOS nanostructures is a common strategy to tune their properties due to their structure-dependent behavior [15,16]. However, among the nanostructures, nanowires (NWs) are the most used ones.

As for the power consumption issue that relates to high operation temperature, when using catalytic NPs, the sensor response to a certain gas can be increased at the same temperature. It means that for the same gas response, the catalytic NPs allows for lowering the

sensor´s operating temperature. When using an integrated micro-heater, it allows for lowering the sensor´s power consumption compared with the one that uses a traditional external heater.

As for the selectivity issue, a common approach is combining several sensors that employ different sensing materials for detection of different gases. Such an approach is used in, for example, so-called electronic noses, which have attracted strong interest of research community [17-19]. Nevertheless, such electronic noses are quite complex, large and expensive. Since it is difficult and very expensive to fabricate a microchip that consists of a number gas sensors with different sensing materials, the selectivity issue can be solved in another way: using the same sensor that operates at different temperatures thanks to the fact that different temperatures activate different gaseous species to react with the sensing material [20-22]. The same result can be achieved by using a sensor chip consisting of several sensors that employ the same sensing material but located at different locations on the chip to exploit the temperature gradient from the same micro-heater as the one described herein.

In this paper, two sensor chips, each consists of four identical resistive sensors (sensor nodes) with on-chip grown SnO_2 NWs bridging the electrodes, were used. The four sensor nodes on each chip were positioned at different distances from the hottest spot of an integrated micro-heater, so that when powering, the nodes obtained their individual operation temperature. Nevertheless, different operation temperatures could only make the nodes more sensitive to one gas than to the other, meaning that the gas selectivity was not of 100 % to one gas and 0% to another. Therefore, a machine learning algorithm (support vector machine) was used in order to distinguish the gas and to estimate its concentration. The SnO_2 NWs on one chip were decorated with Ag NPs, whereas those on the other chip was decorated with Pt NPs. Performance of the two sensor chips and the combination of them were compared.

2. Materials and Methods

2.1. Sensor fabrication

The detailed design of fabricated sensors can be seen in Fig. S1-A and B. Four sensors were integrated at different distances from a resistive microheater. Varying the width of the platinum electrode and the distance from the microheater, different working temperatures were obtained for the various sensor nodes. The structure was optimized using COMSOL Multiphysics® simulations, as shown in Fig. S1-C, with an expected temperature gap of 50-100°C between each subsequent couple of sensors. An infrared thermal emission map of the sensor while supplied with electric power of 170 mW (shown in Fig S1-D) resulted in different working temperatures of 400, 325, 250 and 210°C. Here we name the sensor nodes S1, S2, S3, and S4, with increasing temperature. All metal electrodes and heater on the chips were patterned at the same time using standard lithography, sputter-deposition and lift-off processes. The substrate was made of fused silica glass. Subsequently, a DC sputtering system was used to deposit Cr/Pt/Au/ITO (from bottom to top) layers with a thickness of 5/80/5/20 nm, respectively. The first 5 nm of Cr is used as an adhesion layer in between Pt and glass substrate. The Pt layer is the main part of the electrode that plays a role as conducting and heating material. The ultra-thin layer of Au serves as seeding catalyst for the growth of SnO_2 nanowires using thermal chemical vapor deposition (CVD) method. The top ITO thin layer is aimed to prevent the growing of nanowires over all the Au surface but from the edge. In this study, the SnO_2 NWs were grown by using a thermal CVD system as shown in Fig. S2-A. More specifically, the chips with the patterned electrodes were placed on top of an alumina boat containing Sn powder (99.9%) and they in turn are placed in the middle of the quartz tube. The temperature was increased to 750°C and kept for 10 minutes, while O_2 gas was flowed through the tube at the flow rate of 400 sccm. The furnace was then switched off and cooled down naturally to room temperature. The NWs were grown within a quartz tube

(diameter of 3 cm), 10 cm far from the material source boat. This is a standard recipe in our laboratory, that results in homogenous forests of NWs on substrates of 2x5 cm^2 or more. These specific growth conditions are often repeated for many samples by simply controlling at the temperature, material source, gas flow, and growth duration. A SEM image of the sensor chip with NWs grown is presented in Fig 2S-B and its higher magnification detail, where it is clear that the NWs grew homogenously from the edges of the electrodes. Bridging the sensors electrodes, the NWs connect them from side to side and form the respective sensing resistances.

The surface of the SnO_2 NWs was then decorated with Ag or Pt NPs using DC sputtering at 10 watts, for 40 and 60 seconds, respectively, followed by a heat treatment at 600°C for 4 hours in order to enhance the contact between the metal catalyst NPs and the NWs, and to stabilize the nanostructures.

2.2 Characterization of materials and sensors

Structure, morphology and composition of the Ag and Pt decorated NWs were investigated using X-ray diffraction (XRD, CuKα), field-emission scanning electron microscopy (FE-SEM, Hitachi, S-4800), Energy-dispersive X-ray spectroscopy (EDX), and transmission electron microscopy (TEM, Philips, CM 200).

The gas sensing measurement setup was put in the air-conditioned environment with temperature of about 26°C and humidity of about 50% (as illustrated in Fig. S3). The sensor chip was put inside a 500 ml chamber with the injected gas flowing through a 4 way-valve and exhaust gas evacuated by a vacuum pump. The total gas flow rate was kept at 400 sccm and the gas line outlet was positioned 1 cm away from the multisensor surface. The tested gas concentration was prepared using a mass flow controller setup to dilute the target gas from the

initial concentration (1000 ppm for H_2, 5000 ppm for NH_3, 100 ppm for H_2S, 10000 ppm for Ethanol, and 50000 ppm for Acetone). Here, we used dried air to mix with the target gases at different ratios. The sensor chip inside the chamber was connected to an electronic circuit which collects the sensors signals and sends them to a PC via an Inter-Integrated Circuit (I2C) interface. The transient output voltage from each sensor node was collected from the reference resistances connected in series with the sensor nodes by a home-made data acquisition system. An ATMega 2560 microcontroller was programmed to process the 16-bit analog-to-digital converter (ADS1115), the 8-bit digital-to-analog converter (MAX521) and related electronic components, and send the voltage signal to the PC. This allows to measure a voltage range of 0÷5 VDC with an accuracy of 0.1 mV. The entire system was run by home-built software developed in the Labview environment. A data sampling time of 1 s was set. The concentration values were chosen for each gas in order to include the strictest exposure limit values set by American institutions [23], as can be seen in Table 1.

Table 1: Exposure limits by ACGIH and concentration ranges used in this paper.

Gas	**ACGIH* 8-hour Time Weighted Averages [parts per million, ppm]**	**Test range [ppm]**
Acetone	250	84 – 12600
Ammonia	25	10 – 300
Hydrogen	-	10 – 400
Hydrogen sulfide	1	0.02 – 2.4
Ethanol	1000	30 – 6000

* American Conference of Governmental Industrial Hygienists (ACGIH)

Since the test gases are reducing type, the sensor response was defined as $S=R_a/R_g$, where R_a is the sensor resistance in air and R_g is the sensor resistance in the target gas.

2.3 Machine learning algorithm for gas discrimination and concentration estimate

The responses from the four nodes on the same chip were combined in a 4-dimensional (4D) point for each gas concentration and processed using a support vector machine (SVM) with a linear kernel. A first set of 50 data (4D points) was used to train the system. Another set of 91 data was used to optimize and test its performance. The test concentrations were chosen in between the training concentrations, in order not to overfit the predictive model. In this way, we expect larger errors, which we expect to reflect the sensor's performance under realistic conditions.

3. Results and Discussion

3.1. Characterization of the Ag decorated SnO_2 NWs

Fig. 1a shows a SEM image of the SnO_2 NWs decorated with Ag NPs. The surface of the NW in the foreground shows clearly the presence of numerous Ag NPs. As can be seen, the NWs are quite straight with similar diameters. Analysis of several SEM images showed that the average length of the NWs is 29±11 μm, while their average diameter is 92±42 nm.

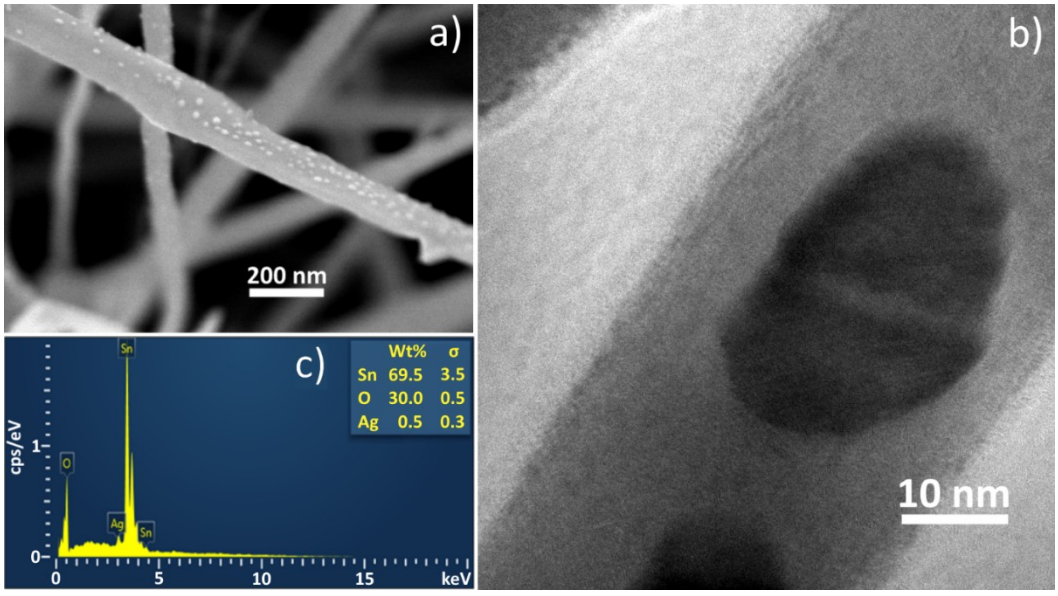

Fig. 1: a) SEM image of Ag decorated SnO_2 NWs; b) TEM image of a NW with an Ag NP on its surface; c) EDX of the elements present in the decorated NWs.

Fig. 1b shows a TEM image of a NW with a couple Ag NPs on its surface. Diameter of the Ag NPs is difficult to estimate since their number in TEM images is too small for a good statistic. The EDX spectrum in Fig. 1c demonstrates that the decorated NWs contain only Sn, O and Ag. As can be seen in the legend, the atomic percentage of Sn and O agrees with the stoichiometry of SnO_2, and the presence of Ag is very small. Notably, the EDX analysis is only qualitative, since references to calibrate it quantitatively were not used.

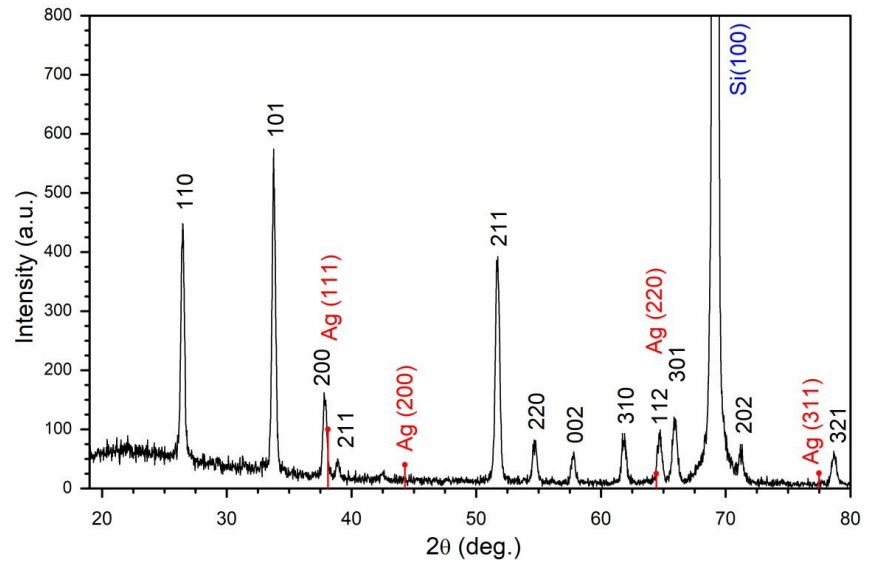

Fig. 2: XRD pattern of the Ag decorated SnO_2 NWs.

The tiny amount of Ag is also reflected in the XRD pattern of the Ag decorated SnO_2 NWs shown in Fig. 2. All peaks in the XRD pattern can be indexed as tetragonal SnO_2 (indexed in black), Ag (indexed in red) or Si (indexed in blue). The calculated lattice parameters of SnO_2 are a = 4.726(1) Å, c = 3.235(1) Å. These values are in good agreement with the reported values (JCPDS file No. 71-0652). No trace of secondary phase is found. The peaks are broad due to the nanosize effect. The strongest peak is Si(100) due to the Si in the substrate, while the four peaks expected from Ag (indexed in red) are almost absent. This is due to two reasons: the tiny amount of Ag, as demonstrated by EDX spectrum in Fig. 1c, and the overlapping of two Ag peaks (including the most intense at 38.1) with those of SnO_2, from

which they could be overwhelmed. These results confirm the elements obtained in Fig. 1.

3.2. Characterization of the Pt decorated SnO_2 NWs

Figure 3a shows a SEM image of the SnO_2 NWs decorated with Pt NPs, which are clearly visible on the surface of the NW in foreground. The average length and diameter of the NWs, estimated from several SEM images is 23±9 μm and 87±38 nm, respectively. The Pt NPs look homogenously dispersed, with widely varied size. The TEM image in Fig. 3b shows a NW with a Pt NP on its surface. The NW is straight and smooth, without any amorphous layer. The EDX spectrum in Fig. 3c shows the elements present in the decorated NWs, namely Sn, O and Pt.

As can be seen in the legend, the ratio between Sn and O is in good agreement with the stoichiometry of SnO_2, while the amount of Pt is small, similarly to the case Ag decorated SnO_2 NWs. Also here, the EDX analysis should be considered only qualitatively.

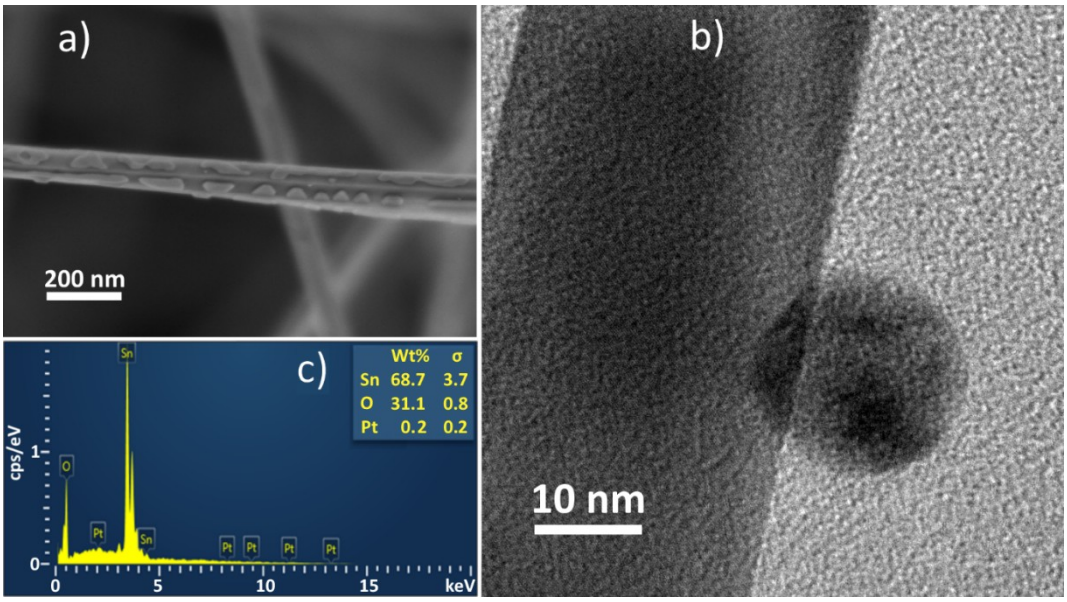

Fig. 3: a) SEM image of Pt decorated SnO_2 NWs; b) TEM image of a NW with Pt NPs on its surface; c) EDX of the elements present in the decorated NWs.

The XRD pattern of the Pt decorated NWs is shown in Fig. 4. Most of the peaks in the

XRD pattern can be indexed as tetragonal SnO_2 (indexed in black), with no trace of secondary phase. Again, the strongest peak is Si(100), due to the Si from the substrate (indexed in blue), which probably overwhelms the Pt peak at 67.5°. The other two Pt peaks are tiny but visible at 39.8 and 46.3°, confirming the results showed in Fig. 3.

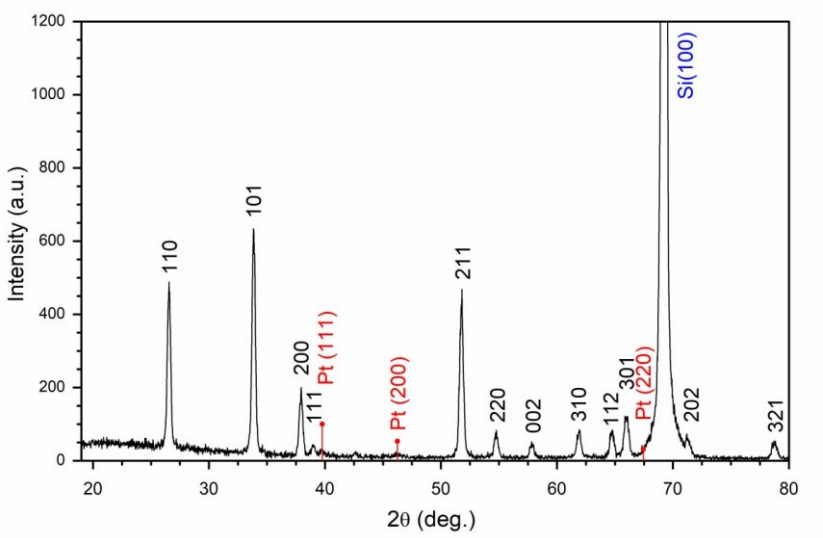

Fig. 4: XRD pattern of the Pt decorated SnO_2 NWs.

3.2. Raw sensor responses, thermal fingerprints and 4D points

The gas sensing characteristics of the sensor chip were measured at a heater power supply of 170 mW. Figure 5A and B show the dynamic voltage of Ag- and Pt decorated SnO_2 NWs chips to H_2S concentrations from 0.02 to 2.4 ppm. Each node of a sensor chip has different gas response characteristics depending on its working temperature (which derives from its distance from the heater). A comparison of Fig. 5A and B clearly shows that the response trend to H_2S gas of Ag decorated sensor chip is totally different from that of the Pt decorated one. For the Ag decorated sensor chip, the highest response was observed at the S1 node, with fast response and recovery times. Meanwhile, the highest H_2S response was achieved from the S3 node for the Pt decorated array. The result is attributed to the different catalytic activity of Ag and Pt nanoparticles towards H_2S.

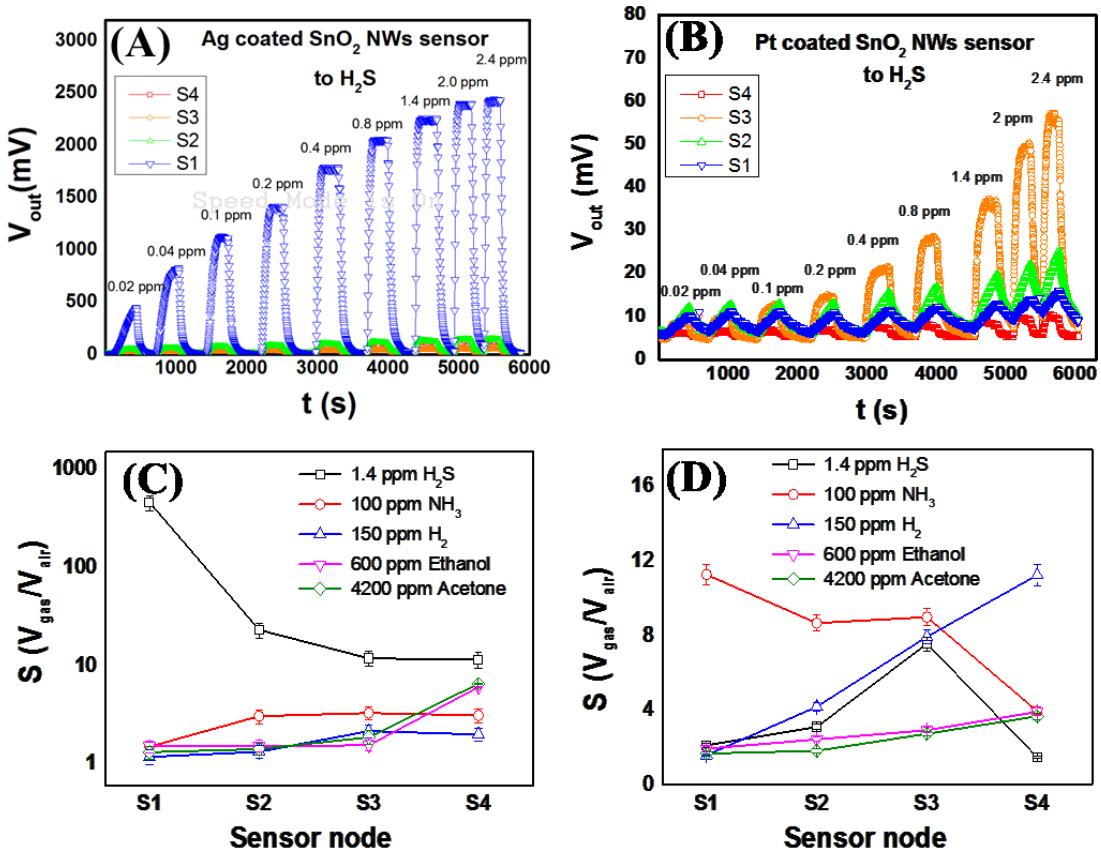

Figure 5. Transient sensor voltage of Ag decorated (A) and Pt decorated (B) SnO_2 NWs sensor chip. Sensor responses to 1.4 ppm H_2S, 100 ppm NH_3, 150 ppm H_2, 600 ppm Ethanol, 4200 ppm Acetone of the sensor nodes in the Ag decorated (C), and Pt decorated (D) SnO_2 NWs sensor chip.

The summary of response from the different sensor nodes of the two chips to the target gases are presented in Fig. 5C (Ag decorated) and D (Pt decorated). From those results, we found that line shapes were different from gas to gas and could be used to distinguish the gases with each sensor chip or their combination. For the Ag decorated SnO_2 NWs, Ag_xO_y nanoparticles might improve the reduction ability of NH_3, H_2, ethanol, and acetone at the increasing of temperature. In contrast, they react much more to H_2S gas at lower working temperature. Also Pt catalyst is efficient towards reducing gases, as well-known [24,25]. Platinum can not only activate the hydrogen atoms in H_2, NH_3, ethanol, and acetone to react to the oxygen radicals adsorbed on SnO_2 NW surface, but it also reacts with hydrogen to form

PtH and PtH_2, causing a change in sensor resistance [26-31]. The efficiency of catalytic ability depends on the binding energy of gas molecules and working temperature of the sensor. For more details about the response and recovery times of the two sensor chips, we provided table S1 (Supplementary Material). The signal to noise ratio (S/N) of the sensor chips are given in table S2 (Supplementary Material). Since the smallest S/N value is 31.7 dB, the calculated gas response data is considered clean and reliable.

Raw voltage signals from the four nodes on each chip were collected at the same time in parallel, under influence of the gases with different concentrations according to Table 2 (see also table 1). The signals were then transformed into traditional gas response data according to the definition in section 2.2, and combined into 4D points. Each very informative 4D point contains four responses and all their correlations. In other words, each 4D point encapsulates a *thermal fingerprint* (response as a function of the working temperature), as previously presented in [32,33].

Table 2. Test concentrations of each gas, in ppm.

Gas	Concentration [ppm]									
Acetone	84	252	420	840	2520	4200	5880	8400	12600	
Ammonia	10	30	50	70	100	150	200	250	300	
Ethanol	30	90	150	300	600	1500	2400	3000	3600	6000
Hydrogen	10	30	50	100	150	200	250	300	350	400
Hydrogen sulfide	0.02	0.04	0.1	0.2	0.4	0.8	1.4	2.0	2.4	

A first set of these 4D points is given to the system with two labels, that is the name of the gas and its concentration. In this way, the system can learn how to recognize each gas, and subsequently estimate its concentration. A support vector machine with a linear kernel was built in Python and used as the "brain" of the system, which uses the training dataset in order to map the 4D space, and then classifies the new data based on that map. In a second step, a support vector regression is used to estimate the concentration of each unknown gas. In Table

2, the concentration values with cyan background are used for train and validation, while those with orange background are used for testing. As can be seen, train and test data were chosen alternately, in order to avoid overfitting.

3.3. t-distributed stochastic neighbor embedding (t-SNE)

Since the data used by the system "brain" are four-dimensional (eight-dimensional when data from two chips are combined), it is not possible to visualize them on screen nor paper. For this reason, an unsupervised method (the data are fed to the system with no label) was used to reduce the dimensionality of the data and allow it to be visualized.

Figure 5 shows the t-SNE projections of the 4D (Fig. 5a and 5b) and 8D (Fig. 5c) data as a visualization support. This algorithm was used because it shrinks the dimensionality while preserving as much variance as possible, and trying to maintain also the local structure of data [34], outperforming other unsupervised parametric dimensionality reduction techniques.

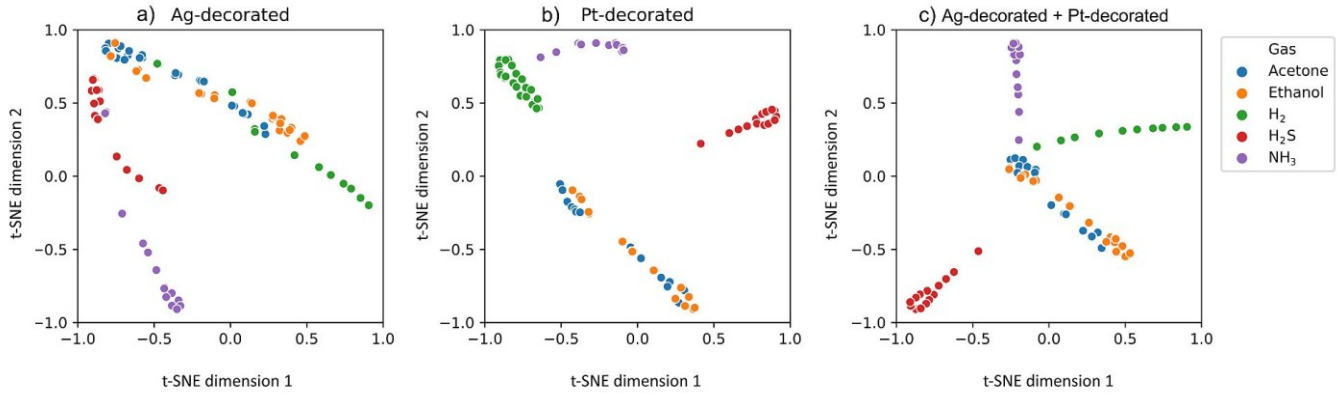

Fig. 6: t-SNE plots showing the relationship among the 4D (a and b) and 8D points (c) relative to the different gases measured by Ag- and Pt decorated sensor chips, and combination of the both, respectively.

This reduced dimension number maximizes the importance of the data along the new directions and helps to better envisage the relationships among the points. It should be noted that the plots in Fig. 5 are not labeled and have no measure units because the coordinates

describe relations among the points, and not absolute or real values, since the mapping is nonlinear.

As mentioned, each point corresponds to a whole chip measurement (4 nodes outputs), or in other words to an entire fingerprint. Each point in Fig. 5 is colored according to the gas it corresponds to, as shown in legend on the right. As can be seen in Fig. 5a, the Ag decorated nodes seem to discriminate the gases only to a certain extent, because acetone, ethanol and H_2 points are overlapping. H_2S and NH_3 are also partially overlapping. Fig. 5b, relative to the Pt decorated sensor nodes, shows a better discrimination, although ethanol and acetone seem to be still confused. The plot in Fig. 5c, relative to the combination of the two sensor chips, shows a good discrimination as well, but also here, ethanol and acetone still overlap in two dimensions. Notably, the "brain" of the system, i.e. the SVM, works in 4D (or 8D), not on these 2D reductions. In fact, it manages to discriminate all the points perfectly, as can be seen in the next sections. The present technique and its plots are used only to give a qualitative idea of the sensor chip performance with unsupervised methods depending only on distances, such as clustering [35,36].

3.4. Classification of gases and estimation of their concentration with Ag decorated sensor chip

As mentioned in section 3.2, an SVM was chosen as chip "brain". Basically, during the training step, five SVM with linear kernels fit the training data (labeled) and split the 4D space in areas belonging to different gases to build a classification model. Subsequently, the position of each new point is compared with the trained model in order to classify it.

As can be seen in Fig. 6a, the confusion matrix has only zeroes out of the diagonal, meaning that there are no misclassifications. Indeed, the Ag decorated chip correctly classified all the 66 points, with an accuracy of 100 %. The X-value (true gas in the measuring

chamber) of each measurement corresponds to its Y-value (classification by the chip). This proves that the SVM, working in the 4D space, discriminates much better than our eyes can do with the only two dimensions in Fig. 5.

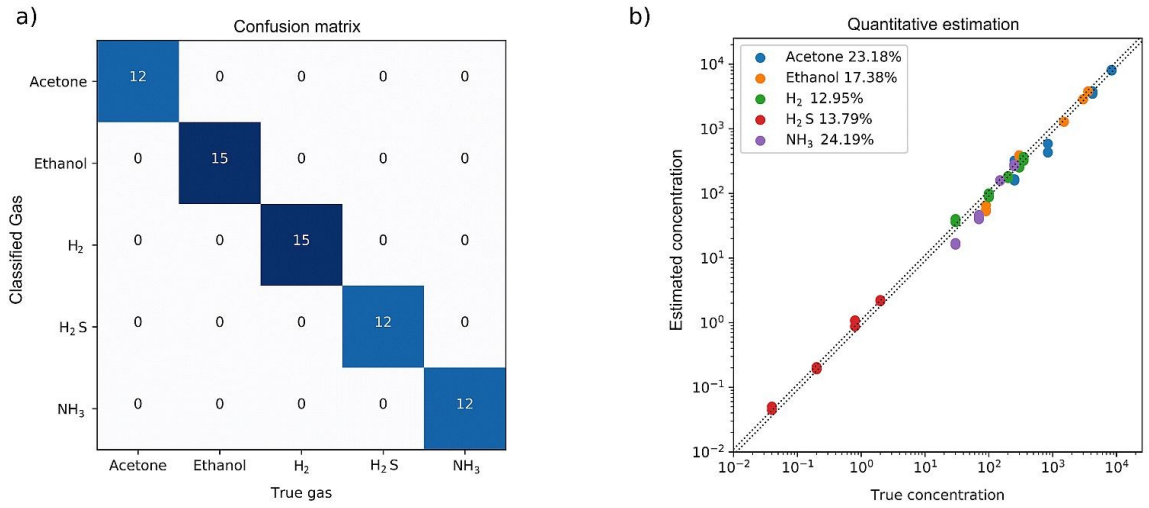

Fig. 7: a) Confusion matrix for the Ag decorated sensor nodes and b) estimated concentrations versus true concentrations for all tested gas. The legend shows the mean absolute percentage error for each set of data.

Indeed, Fig. 6a shows clearly that the SVM algorithm can discriminate very well all the gases tested, even if their concentration ranges are wide and differ from each other. Notably, the test points have been chosen far from the training ones, in order to avoid a possible overfitting. This means that the system is able to understand which gas is present even though it has never tested that gas at that concentration.

In a second step, a support vector regression [37,38] was used to estimate the gas concentrations of the 66 points previously classified and shown in Fig. 6a. An SV regressor was trained for each gas, fitting the training data with their respective concentration labels. On testing data, the regression model was chosen by the SVM classification from the previous step. If the classification was not correct, the wrong model would have been chosen. The results of the SV regression are shown in Fig. 6b, in which each gas is represented by a

unique color. A wrong classification from previous step would result also in a wrong color in this plot. In this type of diagram, the performance of the sensor chip can be easily evaluated with the X axis showing the true concentration and the Y axis showing the estimated concentration. Perfect estimates are found along the diagonal (the estimate of the device corresponds to the concentration of real gas). Train and test data were chosen alternating along each gas range, in order not to overfit the 4D space. This leads to a worse performance (larger error) than that with random-chosen test concentrations, like in a real-world application, but it gives a good idea of the power of this approach. As can be seen in Fig. 6b, the estimation is quite good for all gases at different concentrations (the plot diagonal coincides with the perfect estimate, while the 2 parallel lines show ±10% error). The mean absolute percentage error (MAPE) is calculated for each group of points belonging to one gas, as shown in the legend of Fig. 6b, obtaining: 23.2% for acetone, 17.4% for ethanol, 13.0% for hydrogen, 13.8% for hydrogen sulfide and 24.2% for ammonia. The overall average error of the chip on all the measured gases and concentrations is 18.3%. The errors on the measured gases are quite homogenous, proving that the Ag decorated sensor chip does not work much better for any specific target gas than for the others.

3.5. Classification of gases and estimation of their concentration with Pt decorated sensor chip

The same SVM and the same procedure as in previous section were used here. Also in this case, the chip showed a perfect classification, as illustrated in Fig. 7a, proving that the SVM worked very well with the Pt decorated sensor chip.

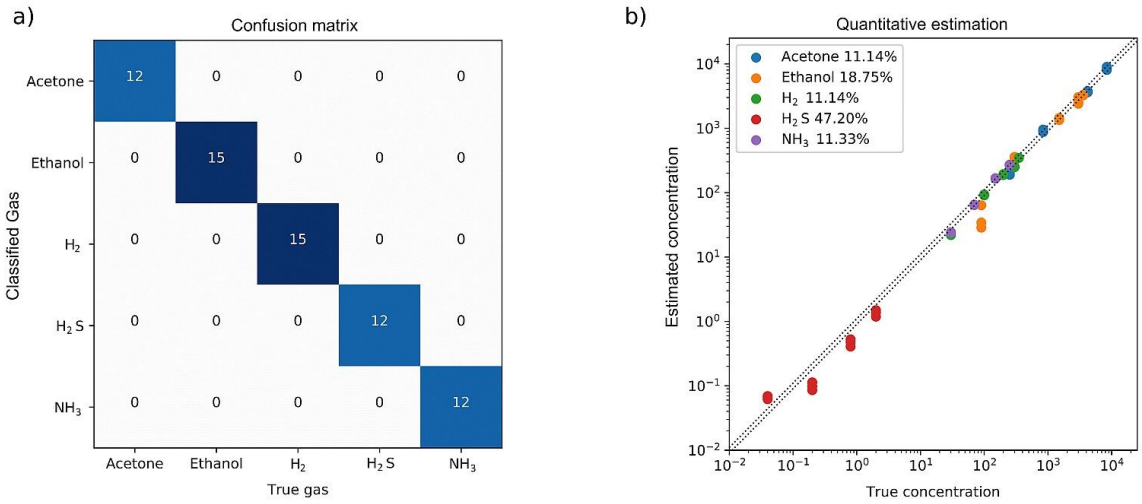

Fig. 8: a) Confusion matrix for the Pt decorated sensor chip and b) estimated concentrations versus true concentrations for all the gas concentrations tested. The legend shows the mean absolute percentage error for each set of data.

The results of the SVM regression are shown in Figure 7b. As can be noticed from the legend, the average errors with the Pt decorated nodes are quite different from those with Ag decorated nodes, namely 11.1% for acetone, 18.8% for ethanol, 11.1% for H_2, 47.2% for H_2S and 9.6% for NH_3. The overall performance is slightly worse, with an average error of 19.5% due to the very high error on H_2S. Apart from H_2S, the Pt decorated nodes shows errors quite similar to those with Ag decorated nodes for ethanol and H_2, but more than twice better for acetone and NH_3. However, it should be noted that the H_2S concentration range is much lower than that of the other gases (Table 2), implying that it is more difficult to measure this gas accurately.

3.6. Classification of gases and estimation of their concentration with Ag and Pt decorated sensor chips combined

The outputs of the two sensor chips (4 responses from the Ag decorated nodes and 4 responses from the Pt decorated nodes) were combined in order to compare their performance

with that of each device separately. The confusion matrix of this combined sensing system is shown in Fig. 8a.

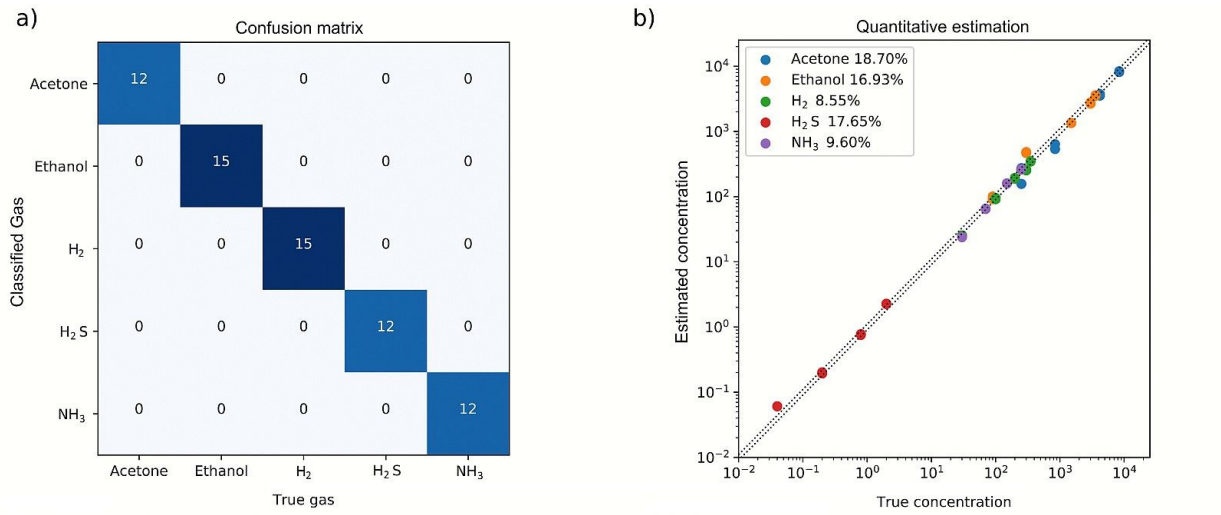

Fig. 9: a) Confusion matrix for the Ag decorated combined with the Pt decorated sensor chip and b) estimated concentrations versus true concentrations for all the gas concentrations of test gases. The legend shows the mean absolute percentage error for each set of data.

As expected, the classification combining the two chips is perfect for all 66 test points. The estimation of concentrations given in Fig. 8b looks very good too, with few points outside the diagonal lines. In detail, the MAPE values (in the legend) for the different gases are 18.7% for acetone, 16.9% for ethanol, 8.6% for H_2, 17.7% for H_2S and 9.6 % for NH_3. It is clear that in this case the chips together work better for H_2 and NH_3 than for the other gases. The average error of 14.3 % is better than that of each chip separately.

The comparison of the Ag decorated sensor chip, the Pt decorated sensor chip and their combination is summarized in Fig. 9. As can be seen, the performance of the Ag decorated sensor chip is more homogeneous and has the best error for H_2S. On the other hand, the Pt decorated sensor chip is very bad for H_2S but is much better than its Ag decorated counterpart for acetone, H_2 and NH_3. The performance of the two combined sensor chips is in general better than that of each separately. The average error is in fact 14.3 % in this case, compared

with 19.9 % and 18.3 % of the chips separately.

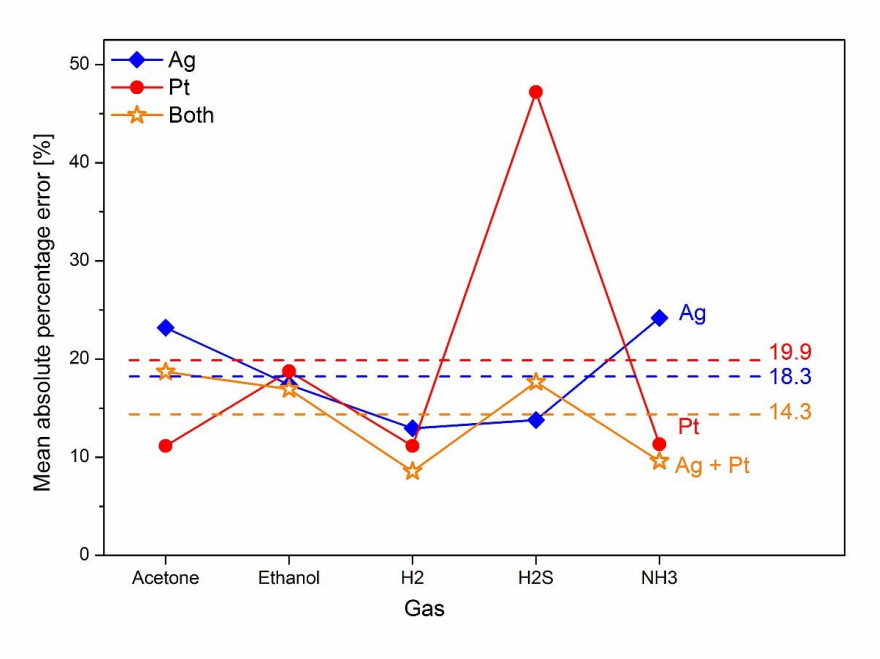

Fig. 10: Mean absolute percentage error towards each gas for Ag decorated sensor chip, Pt decorated sensor chip and their combination.

These results prove that using a multi-sensor based on only one single nanomaterial as sensing material and thermal gradient represents a good approach to improve selectivity. It may not yet compare to the performance of an electronic nose that employs several materials (metal oxides, organic molecules, polymers…), but it possesses already many superior advantages such as simplicity, small-size, light weight, and low-cost and low power consumption. Furthermore, when using this approach, an appropriate selection of the nanomaterial for sensing of certain target gases is more important than using a combination of different nanomaterials or a large number of sensor nodes, as in the case of electronic noses.

4. Conclusions

Two multi-sensor chips using SnO_2 NWs decorated with Ag and Pt NPs and their

combination were used as chemoresistive sensors to distinguish 5 different reducing gases (acetone, ammonia, ethanol, hydrogen and hydrogen sulfide) and to measure their concentrations. Each sensor chip is composed of four integrated sensor nodes working along a thermal gradient, and the four responses from them are combined in 4D points. A first dataset of 4D points is used to train the system "brain" (based on SVM machine learning algorithm), whereas any following point is used to test the sensor performance. Both Ag and Pt decorated sensor chips and their combination achieved a perfect classification (100%). Nevertheless, the Ag decorated sensor chip show a slightly better overall performance than that of the Pt decorated ones (average error 18.3% and 19,9%, respectively), while their combination displays considerable better overall performance than the single chips (average error 14.3%). These results are very good, especially considering the merits of this approach (small size and weight, simplicity, low cost and consumption) which are the hard requirements of portable and wearable gas sensing systems.

Acknowledgements

This work was financially supported by the Ministry of Science and Technology, under the Grant No. ĐTĐLCN.21/17.

References

[1] D. Barreca, A. Gasparotto, F. Gri, E. Comini, C. Maccato, Plasma-Assisted Growth of β–MnO2 Nanosystems as Gas Sensors for Safety and Food Industry Applications, Adv. Mater. Interfaces 5 (2018) 1800792.

[2] A.A.Makky, A.Alaswad, D. Gibson, A.G.Olabi, Renewable energy scenario and environmental aspects of soil emission measurements, Renewable Sustainable

Energy Rev. 68 (2017) 1157–1173.

[3] Y. Ge, Z. Wei, Y.-S.Li, J. Qu, B.-Y.Zu, X-C.Dou, Highly sensitive and rapid chemiresistive sensor towards trace nitro-explosive vapors based on oxygen vacancy-rich and defective crystallized In-doped ZnO, Sens. Actuators B 244 (2017) 983–991.

[4] M. Righettoni, A. Amann, S.E. Pratsinis, Breath analysis by nanostructured metal oxides as chemo-resistive gas sensors, Mater. Today 18 (2015) 163-717.

[5] Y. Xia, P. Yang, Y. Sun, Y. Wu, B. Mayers, B. Gates, Y. Yin, F. Kim, H. Yan, One-Dimensional Nanostructures: Synthesis, Characterization, and Applications, Adv. Mater. 15 (2003) 353-389.

[6] E. Comini, C. Baratto, G. Faglia, M. Ferroni, A. Vomiero, G. Sberveglieri, Quasi-one dimensional metal oxide semiconductors: Preparation, characterization and application as chemical sensors, Progress in Materials Science 54 (2009) 1–67.

[7] K. Nguyen, C.M. Hung, T.M. Ngoc, D.T. Thanh Le, D.H. Nguyen, D. Nguyen Van, H. Nguyen Van, Low-temperature prototype hydrogen sensors using Pd-decorated SnO_2 nanowires for exhaled breath applications, Sens. Actuators B 253 (2017) 156-163.

[8] A. Katoch, S-.W- Choi, G.-J. Sun, S.S. Kim, Low temperature sensing properties of Pt nanoparticle-functionalized networked ZnO nanowires, J. Nanosci. Nanotechnol. 15 (2015) 330-333.

[9] I.S. Jeon, G. Bae, M. Jang, W. Song, S. Myung, S.S. Lee, H.-K. Jung, J. Hwang, K.-S. An, A synergistic combination of zinc oxide nanowires array with dual-functional zeolitic imidazolate framework-8 for hybrid nanomaterials-based gas

sensors, Compo. Part B-Eng. 180 (2020) 107552.

[10] J. Hu, M. Chen, Q. Rong, Y. Zhang, H. Wang, D. Zhang, X. Zhao, S. Zhou, B. Zi, J. Zhao, J. Zhang, Z. Zhu, Q. Liu, Formaldehyde sensing performance of reduced graphene oxide-wrapped hollow SnO_2 nanospheres composites, Sens. Actuators B 307 (2020) 127584.

[11] Q. Simon, D. Barreca, A. Gasparotto, C. Maccato, E. Tondello, C. Sada, E. Comini, A. Devi, R. Fischer, Ag/ZnO nanomaterials as high performance sensors for flammable and toxic gases, Nanotechnology 23 (2013) 025502.

[12] C.S. Prajapati, S. Benedict, N. Bhat, An ultralow power nanosensor array for selective detection of air pollutants, Nanotechnol. 31 (2019) 025301.

[13] T.M. Ngoc, N.V. Duy, C.M. Hung, N.D. Hoa, H. Nguyen, M. Tonezzer, N.V. Hieu, Self-heated Ag decorated SnO2 nanowires with low power consumption used as a predictive virtual multisensor for H_2S-selective sensing, Anal. Chim. Acta 1069 (2019) 108-116.

[14] S. Khaldi, Z. Dibi, Neural network technique for electronic nose based on high sensitivity sensors array, Sensing and Imaging 15 (2019) 15.

[15] B.-Y.Wang,D.-S.Lim, Y.-J. Oh, CO gas detection of Al-doped ZnO nanostructures with various shapes, Jpn. J. Appl. Phys. 52 (2013) 101103.

[16] M.Tonezzer, T.T.L. Dang, N. Bazzanella, V.H. Nguyen, S. Iannotta, Comparative gas-sensing performance of 1D and 2D ZnO nanostructures, Sens. Actuators B 220 (2015) 1152–1160.

[17] E.N. Carmona, V. Sberveglieri, A. Ponzoni, V. Galstyan, D. Zappa, A. Pulvirenti, E. Comini, Detection of food and skin pathogen microbiota by means of an

electronic nose based on metal oxide chemiresistors, Sens. Actuators B 238 (2017) 1224–1230.

[18] H.G. Moon, Y. Jung, S.D. Han, Y.-S.Shim, B. Shin, T. Lee, J-S. Kim, S. Lee, S.C. Jun, H.-H. Park, C. Kim, C-Y.Kang, Chemiresistive electronic nose toward detection of biomarkers in exhaled breath, ACS Appl. Mater. Interfaces 8 (2016) 20969-20976.

[19] S. Jiang, J. Wang, Y. Wang, S. Cheng, A novel framework for analyzing MOS E-nose data based on voting theory: Application to evaluate the internal quality of Chinese pecans, Sens. Actuators B 242 (2017) 511–521.

[20] M. Tonezzer, D.T.T. Le, T.Q. Huy, S. Iannotta, Dual-selective hydrogen and ethanol sensor for steam reforming systems, Sens. Actuators B 236 (2016) 1011–1019.

[21] M. Tonezzer, L.T.T. Dang, H.Q. Tran, S. Iannotta, Multiselective visual gas sensor using nickel oxide NWs as chemiresistor, Sens. Actuators B 255 (2018) 2785–2793.

[22] M. Tonezzer, Selective gas sensor based on one single SnO_2 NW, Sens. Actuators B, 288 (2019) 53-59.

[23] https://www.osha.gov/dsg/annotated-pels/index.html

[24] I. S. Hwang et al., “Enhanced H2S sensing characteristics of SnO2 nanowires functionalized with CuO,” Sensors Actuators, B Chem., vol. 142, no. 1, pp. 105–110, 2009.

[25] P. S. Kolhe, P. M. Koinkar, N. Maiti, and K. M. Sonawane, “Synthesis of Ag doped SnO2 thin films for the evaluation of H2S gas sensing properties,” Phys. B Condens. Matter, vol. 524, no. July, pp. 90–96, 2017.

[26] A. Dedieu, “Theoretical studies in palladium and platinum molecular chemistry,” Chem. Rev., vol. 100, pp. 543–600, 2000.

[27] D. Degler, H. W. Pereira de Carvalho, K. Kvashnina, J.-D. Grunwaldt, U. Weimar, and N. Barsan, “Structure and chemistry of surface-doped Pt:SnO2 gas sensing materials,” RSC Adv., vol. 6, no. 34, pp. 28149–28155, 2016.

[28] L. Bizhou, F. Jia, B. Lv, Z. Qin, P. Liu, and Y. Chen, “Facile synthesis and remarkable hydrogen sensing performance of Pt-loaded SnO2hollow microspheres,” Mater. Res. Bull., vol. 106, no. November 2017, pp. 403–408, 2018.

[29] I. H. Kadhim, H. Abu Hassan, and Q. N. Abdullah, “Hydrogen gas sensor based on nanocrystalline SnO2 Thin Film grown on bare Si substrates,” Nano-Micro Lett., vol. 8, no. 1, pp. 20–28, 2016.

[30] Q. N. Abdullah, F. K. Yam, J. J. Hassan, C. W. Chin, Z. Hassan, and M. Bououdina, “High performance room temperature GaN-nanowires hydrogen gas sensor fabricated by chemical vapor deposition (CVD) technique,” Int. J. Hydrogen Energy, vol. 38, no. 32, pp. 14085–14101, 2013.

[31] S. Dhall and N. Jaggi, “Room temperature hydrogen gas sensing properties of Pt sputtered F-MWCNTs/SnO2 network,” Sensors Actuators, B Chem., vol. 210, pp. 742–747, 2015.

[32] M. Tonezzer, T.T.L. Dang, Q.H. Tran, V.H. Nguyen, S. Iannotta, Selective hydrogen sensor for liquefied petroleum gas steam reforming fuel cell systems, Int. J. Hydrogen Energy 42 (2017) 740-748.

[33] M. Tonezzer, J.-H. Kim, J.-H. Lee, S. Iannotta, S.S. Kim, Predictive gas sensor based on thermal fingerprints from Pt-SnO2 NWs, Sens. Actuators B 281 (2019) 670-678. DOI: 10.1016/j.snb.2018.10.102.

[34] L. van der Maaten, G. Hinton, Visualizing data using t-SNE, J. Mach. Learn. Res. 9 (2008) 2579-2605.

[35] J. Mao, Y. Lu, N. Chang, J. Yang, S. Zhang, Y. Liu, Multidimensional colorimetric sensor array for discrimination of proteins, Biosens. Bioelectron. 86 (2016) 56–61.

[36] M. Mahmoudi, S.E. Lohse, C.J. Murphy, K.S. Suslick, Identification of nanoparticles with a colorimetric sensor array, ACS Sens. 1 (2016) 17–21.

[37] S. Xu, X. An, X. Qiao, L. Zhu, L. Li, Multi-output least-squares support vector regression machines, Pattern Recognit. Lett.34 (2013) 1078–1084.

[38] M. Tonezzer, D.T.T. Le, S. Iannotta, N.V. Hieu, Selective discrimination of hazardous gases using one single metal oxide resistive sensor, Sens. Actuators B, 277 (2018) 121-128.